J Nanostruct Chem (2015) 5:85–94
DOI 10.1007/s40097-014-0139-5

ORIGINAL

Green synthesis and growth kinetics of nanosilver under bio-diversified plant extracts influence

Enock Olugbenga Dare · Charles Ojiefoh Oseghale · Ayomide Hassan Labulo · Elijah Temitope Adesuji · Elias Emeka Elemike · Jude Chinedu Onwuka · Janet Titilayo Bamgbose

Received: 23 August 2014 / Accepted: 15 November 2014 / Published online: 18 December 2014

Abstract In this report, synthesis, growth and formation kinetics of silver nanoparticles mediated by various plant extracts in their biodiversity have been monitored using UV–Vis spectrophotometer by sampling at time intervals during bioreduction process. Plasmon band resonance of the silver nanoparticles was observed as the reaction progresses indicating nucleation and particle formation. There were cases of red shifting indicating particle size increase. In the bioreduction process, onset of nanoparticle nucleation and growth were observed within 2, 5, 10 or 30 min and eventual formation of spherical or quazi-spherical amidst twinned morphology as determined by transmission electron microscope (TEM). The nanosilver growth kinetics mechanism has been probed using a time-resolved UV–Vis in conjunction with TEM following existing Lifshitz–Slyozov–Wagner theory. For some biological extract-mediated synthesis, a single-stage mechanism that is diffusion controlled following Ostwald ripening (OR) is proposed. Whereas, for other bioreduction process, a double stage involving (1) initial OR followed by (2) surface adsorption-oriented attachment is proposed for temporal evolution of the nanosilver in green environment.

E. O. Dare · C. O. Oseghale · A. H. Labulo · E. T. Adesuji · E. E. Elemike · J. C. Onwuka
Department of Chemistry, Federal University Lafia, Lafia, Nigeria

E. O. Dare · J. T. Bamgbose
Department of Chemistry, Federal University of Agriculture Abeokuta, Abeokuta, Nigeria

E. E. Elemike (✉)
Department of Chemistry, Federal University of Petroleum Resources Effurun, Warri, Nigeria
e-mail: chemphilips@yahoo.com

Keywords Silver nanoparticles · Ostwald ripening · Oriented attachment · Growth kinetics · Green system · UV–Vis spectroscopy

Introduction

Nanocrystalline silver particles have found tremendous applications in the field of highly sensitive biomolecular detection, diagnostics, antimicrobial (antibacterial) activities, photocatalysis and lithography [1–4].

In the global efforts to reduce generated hazardous waste, "green" chemistry and chemical processes are progressively integrating with modern developments in science and industry [5]. Various approaches using plant extracts have been used for the synthesis of silver nanoparticles. These approaches have many advantages over chemical, physical, and microbial synthesis because there is no need of the elaborated process of culturing and maintaining the cell, using hazardous chemicals, high-energy and wasteful purifications [6]. Researchers are exploiting this avenue and have reported the synthesis of silver nanoparticle (SNP) using plant extracts such as *Jatropha curcas* seed, bitter apple, neem leaf, green tea, *Sphaeranthus amaranthoides*, *Wrightia tinctoria* leaves, *Datura metel* flower [7–13].

It has been elucidated that biomolecules with carbonyl, hydroxyl, and amine functional groups have the potential for metal ion reduction and capping of the newly formed particles during their growth processes [7, 14].

Biomolecules in plants and spices extract are essential oils (terpenes, eugenols, etc.), polyphenols, carbohydrates, etc. These compounds contain active functional groups, such as hydroxyl, aldehyde, amine and carboxyl units, which may play important role in the reduction and stabilization of Ag^{+} to Ag^{0}.

In this report, we have engaged biodiversity plants extract that are peculiar to Nigeria for the synthesis of silver nanoparticles (SNPs). The plants include *Afromomum melegueta* (Am), *Anacardium occidentale linn* (Ao), *Capsicum chinense* (Cc), *Citrus aurantifolia* (Ca), *Ocimum gratissimum* (Og), *Newbouldia laevis* (Nl), *Piper guineense* (Pig), *Psidum guajava* (Pg), *Gangronema latifolum* (Gl), *Telfairia occidentalis* (To), *Xylopia aethiopica* (Xa) and *Vernonia amygdalina* (Va). Most of these plants extract have been well studied with their physiochemical, phytochemical, cytotoxic and pharmacological properties discussed [15–22].

The synthetic approaches for preparing nanoscale materials are various and mainly include chemical method, physical techniques and biological means [23–25]. Recently, our group applied the biological means in synthesizing SNPs using pineapple leaf [26].

The study on the crystal growth is important for the full understanding of size and shape formation especially for nanostructured system synthesized by chemical method. However, at the moment, information and knowledge of the growth kinetics of biological process initiated by plant extracts, following solution phase procedure is obviously in a state of obscurity. The growth process in wet chemical procedure has often been discussed in terms of Ostwald ripening (OR) process, based on the common belief that such growth in nanomeric regime proceeds via a diffusion-controlled ripening process.

However, recent theoretical [27] as well as experimental studies [28] suggest that the growth of nanoparticles can be significantly influenced by the rate of surface reactions, thereby showing departure from the diffusion-limited growth behaviour leading to the newly developed oriented attachment (OA) mechanism [27–29].

Therefore, in this report, we focus on the synthesis of SNPs via various biodiversified plant extracts. The nanoparticle growth kinetics have been probed from the bioprocessed solution in a time-resolved UV–Visible spectroscopy complemented by TEM using the existing coarsening and particle growth mechanism as template.

Methodology

Materials

Am, Cc, Ca Og, Nl, Pig, Pg, Gl, To, Xa, Va, Ao plant extracts were used. $AgNO_3$ was commercially obtained from Sigma-Aldrich.

Preparation of extract

Twelve plant leaves and spices (Table 1) were obtained from Lafia, Nasarawa State, Nigeria. The leaves were washed, air dried and chopped. Extractions of the active reduction-capable biomolecules were done using water (1:10 v/v) and filtered. The filtrates were kept for further use at 40 °C. The same procedure was adopted for every individual plant used in this work.

Synthesis and characterization of silver nanoparticles

The filtrate (5.0 ml each) was added to 20 ml of 1 mM $AgNO_3$ solution. The resulting solution was heated at 70 °C for 30 min. Aliquot sample of the mixture was taken at intervals (2, 5, 10, 15 and 30 min) and rate of the reduction of Ag^+ ions to Ag^0 monitored by measuring the absorbance or appearance of plasmon bands with T60 UV–Vis Spectrophotometer [26]. During characterization and monitoring, we engaged the time-resolved absorption spectra of the UV–Vis spectroscopy in probing the growth kinetics of SNPs in bioprocessed solution. Morphology and

Table 1 A compendium of the plants used for silver nanoparticles synthesis

S/N	Botanical name	Common name	Local (Igbo) name	Family name	Part of the plant used
1	*Afronomum melegueta (Am)*	Aligator pepper	Ose oji	Zingiberaceae	Seed
2	*Anacardium occidentale linn* (*Ao*)	Cashew	Kashuu	Anarcadiaceae	Leaf
3	*Psidium guajava* (*Pg*)	Guava	Gova	Myrtaceae	Leaf
4	*Ocimum gratissimum* (*Og*)	Scent leaf	Nchuawu	Labiateae	Leaf
5	*Newbouldia laevis* (*Nl*)	–	Ogirisi	Bignoniaceae	Leaf
6	*Telfairia occidentalis* (*To*)	Fluted pumpkin	Ugu	Cucurbitaceae	Leaf
7	*Gangronema latifolium* (*Gl*)	–	Utazi	Asclepiadaceae	Leaf
8	*Piper guineense* (*Pig*)	–	Uziza	Piperaceae	Leaf
9	*Citrus aurantifolia* (*Ca*)	Lime	Oroma nkirisi	Rutaceae	Leaf, peels
10	*Vernonia amygdalina* (*Va*)	Bitter leaf	Onugbu	Asteraceae	Leaf
11	*Xylopia aethiopica* (*Xa*)	Black pepper	Uda	Annonaceae	Seed
12	*Capsicum chinense* (*Cc*)	Red pepper	Ose ocha	Solanaceae	Stalk

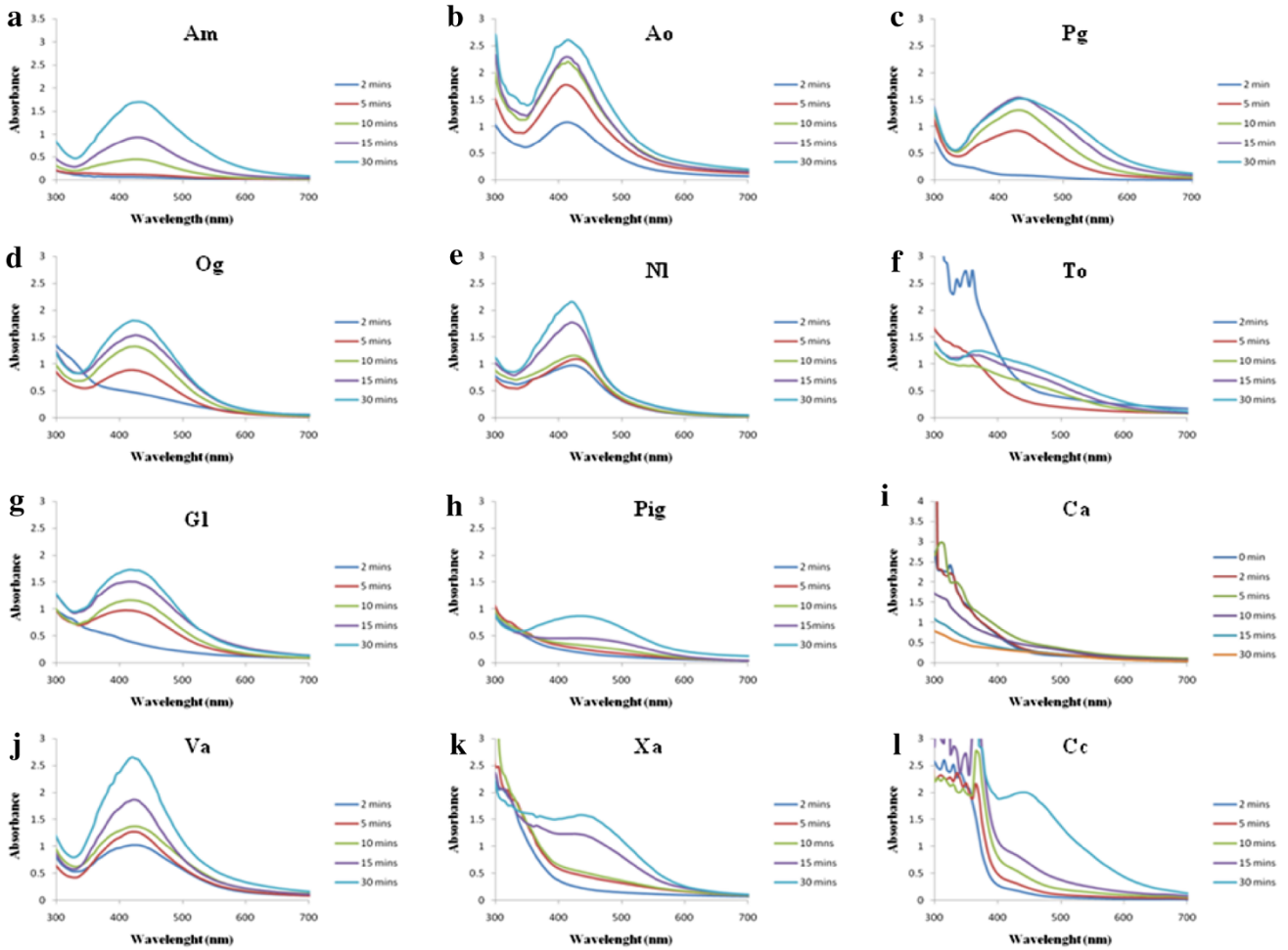

Fig. 1 **a–l** Time-resolved PBR spectrum of silver nanoparticles (SNPs) obtained from various plant extracts

sizes of SNPs obtained from green system were obtained from Transmission electron microscope (TEM). It should be noted that representative plots are only provided. Other plots are not included for brevity and scaling convenience. X-ray diffraction (XRD) analysis of the SNPs obtained is the same [26]. Rate constants of every bioreduction process were determined from the time-resolved UV–Vis results following Beer–Lambert law and first-order equation (log $(A_\infty - A_t) = \log (A_\infty - A_o) - kt/2.303$.

Results and discussion

Synthesis and monitoring of SNPs growth

The world of science globally is working towards a sustainable and ecofriendly future. With such a growing need to minimize or eliminate the use of environmental-risk substances as the green chemistry principle described [30], we have engaged our local biodiversity plant extracts in the synthesis of silver nanoparticles (SNPs) under a time-resolved UV–Vis monitoring.

In most cases, the reaction between biological extracts and $AgNO_3$ solution indicate colour changes in a manner similar to previous work [26]. The colour change is due to characteristic vibrations due to changes in electronic energy levels. However, Ca and To initiated reaction did not display colour changes. No characteristic plasmon band resonance (PBR) peak was observed. This is an indication that these plant extracts are not significant for SNPs synthesis due to high acidity level and insufficient amount of reductive biomolecules for Ag^+ reduction. Among all the extracts used for the synthesis, Pg, Ao, Nl and Xa exhibited unprecedented bioreduction properties by effecting nucleation and growth of SNPs within 2 min of reaction (Fig. 1b, c, e, k; Table 2). In particular for Pg-mediated (Fig. 1c) synthesis, there is spectra overlap at the 15th and 30th min with no further changes in intensity and sizes. This is an indication that reaction was completed within 15 min. This is, indeed, a remarkable experimental

Table 2 The growth kinetics parameters of the bioreduction process

S/N	Names of leaves	Minimum SNP growth time (min)	Maximum intensity at 30 min	Average size	Wavelength (nm)	Rate constant ($\times 10^{-1}$ s^{-1})	Proposed mechanism
1	*Afronomum melegueta*	10 (size 7.6 nm)	1.706	27	430	2.6	OR → OA
2	*Anacardium occidentale* Linn.	2 (size 3.2 nm)	2.587	9	410	13.1	OR
3	*Psidium guajava*	2	1.525	14	430	8.9	OR
4	*Ocimum gratissimum*	5	1.807	19	420	4.7	OR → OA
5	*Newbouldia laevis*	2	2.163	8	420	11.9	OR
6	*Telfairia occidentalis*	–	–	–	–	–	–
7	*Gangironema latifolium*	5	1.735	17	415	3.8	OR
8	*Piper guineense*	15	0.872	33	435	1.5	OR
9	*Citrus aurantifolia* (leaf)	–	–	–	–	–	–
10	*Xylopia aethiopica*	2	2.659	9	420	13.8	OR
11	*Capsicum chinense*	15	1.584	41	440	1.8	OR → OA
12	*Vernonia amygladina*	30	2.006	53	440	1.6	OR → OA

observation in the reported history of green synthesis. The broadening of the peaks shows that the particles are polydispersed [31].

In the case of Og and Gl-influenced synthesis, particle growth started after 5 min and continued. However, Va did not support SNP synthesis until the 30th min of reaction with accompanied PBR widening. SNPs growth onset of 15 min was observed for both Pig and Cc-mediated reaction, though in a slow growing style suggesting different peculiar mechanistic character towards particle formation. The red shifting observed in the PBR of some of the extracts (Am, Pg, Pig, Cc and Va) used for the synthesis is an indication of size increment as a consequence of biomolecular-capped SNP which has been noted for its application in optical materials [32, 33]. Cases where occurrence of fast particle growth was observed have been attributed to the plant extracts possessing requisite optimum bioreducing agents as previously detailed [19, 20]. The slow growing style of some SNP as evident in their respective PBR could be attributed to strong interactions between the biomolecules and the growing silver particles which seem to be isotropic as it is time dependent [34].

In plant-mediated synthesis, the control of the size of SNPs has been proposed to be time-dependent reaction [35]. Basically, the longer the reaction time the larger the sizes. Most of the bioreduction process adopted in this work with the exception of Pg-influenced synthesis followed this pattern. As seen in Table 2, nucleation and growth onset (2 min) for Ao, Pg, Nl and Xa bioreduction are short timed compared with others that emanated from Am, Cc, Pig and Va whose nucleation and growth onset were observed at 10, 15 and 30 min, respectively. Consequently, the average particle sizes obtained under Ao, Pg, Nl and Xa-mediated synthesis are 9, 14, 8 and 19 nm, respectively while the sizes under Am, Cc, Pig and Va influence fall in the average sizes of 27, 41, 33 and 51 nm, respectively (Table 2).

Figure 2 present plots of the plasmon intensity against maximum reaction time for every bioreduction process, from their corresponding UV–Vis graphs in Fig. 1a–l. Apparently, in most cases, the plasmon intensity at the reaction time of 15 min is close to that at 30 min, meaning completion of reaction on or before 30 min. However, Ao and Xa-influenced reaction have SNPs plasmon intensity highest and supported with highest reaction rate and smallest nucleation/growth onset time. These results underscore the significance and broader plane of functionalities in Ao and Xa among other plant extracts.

Figure 3 displays typical XRD patterns of the nanosilver particles obtained from Ao and Am-mediated synthesis at the initial nanoparticle formation onset time of 2 and 10 min, respectively. Regardless of variation in nanoparticle formation onset time, a number of Bragg reflections with 2θ values of 38.13°, 46.19°, 63.42° and 77.17° corresponding to the (111), (200), (220) and (311) sets of plane lattice are apparently observed in both Ao and Am-mediated synthesis and which may be indexed as the band for face-centred cubic structure of silver. These results attest to crystallinity nature of the SNPs.

However, at these presumably growth onset time (Table 2), Ao and Am gave nanoparticles sizes of 3.2 and 7.6 nm, respectively.

In comparison, Ao-influenced synthesis at smaller growth onset time displays broader peaks and smaller nanosilver size with characteristic higher intensity (1.1) compared with that of Am-influenced intensity (0.49). These results reflect that the smaller the nanoparticle sizes, the higher the intensity. This trend is maintained as the reaction progresses to 30 min.

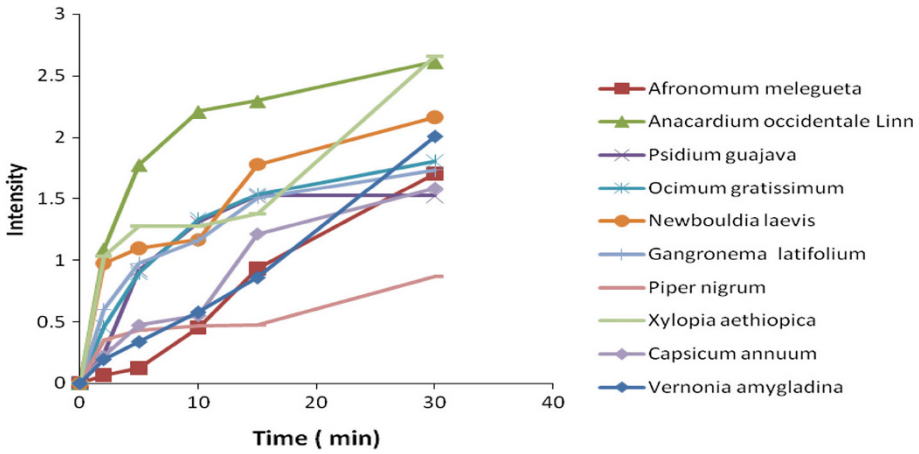

Fig. 2 Plots of the intensity of PBR against reaction time for silver nanoparticles as obtained from various plants extracts

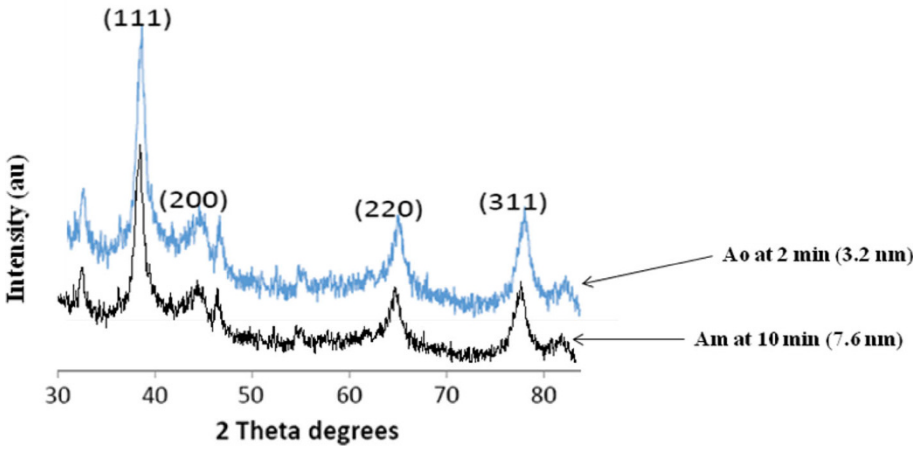

Fig. 3 XRD diffraction patterns for nanosilver particles as mediated by Ao and Am plants extracts at different nanoparticles formation onset time

Therefore, for these two plant extracts (Ao and Am), as example, peak width of Am-mediated synthesis is smaller and narrower corresponding to an increased nanoparticle size.

Figure 4a–d displays the nanoparticle size progression with time (bold arrow indicates direction), for example, for Ao and Am bioreduction processes at initial nanoparticle formation stage and final stage (30 min). Images in Fig. 4a, b were obtained at the initial 10 min nanoparticle formation time and 30 min reaction completion time, respectively for Am-influenced system. Images in Fig. 4c, d were obtained at the initial 2 min and final stage (30 min) for Ao-influenced system. In both mediated cases, nanoparticle size increase with increasing reaction time regardless of the differences in nucleation or coarsening period. The same trends obtained for Ao system are repeated for Pg, Nl, Gl, Pig and Xa-mediated system producing spherical morphology as seen in Fig. 4c, d. These time-dependent features leading to nanoparticles of varying sizes are characteristic of isotopic growth of spherical morphologies [36]. Scenario displayed for Am system are similarly reflected in other Og, Cc and Va bioreduction processes leading to combination of quazi and twinned morphologies (Fig. 4a, b). Moreover, this irregularity in shapes obtained in Am series and in particular, at reaction completion stage (Fig. 4b) may be seen as a consequence of epitaxial attachment either from primary nanoparticles initially formed [34] or organic from plant extracts [28].

Incidentally, morphology variation is based on the fact that most of the plant extracts used are phytochemically rich containing varying proportion of the bioreducing biomolecules except *To* and *Ca*. Indeed, the interaction between the biomolecules (phenolics, flavonoids, terpenoids etc.) and the metal atoms is the underlining factor that supports SNP nucleation and formation.

It is noteworthy that plant extracts initiated nucleation and growth of the SNP at different rate. Rate constant for every bioreduction was calculated from UV–Vis data. Xa and Ao produced SNP following relatively high rate constant of 13.8×10^{-1} s^{-1} and 13.1×10^{-1} s^{-1}, respectively. The relatively higher rate constant exhibited by Xa, Ao, Pg and Nl is an index of requisite optimum bioreducing molecule in the plant extracts that brought about a fast reaction leading to 2 min nucleation onset time. However, Og, Gl, Pig, Cc and Va have lower rate constant supported by longer nucleation onset time.

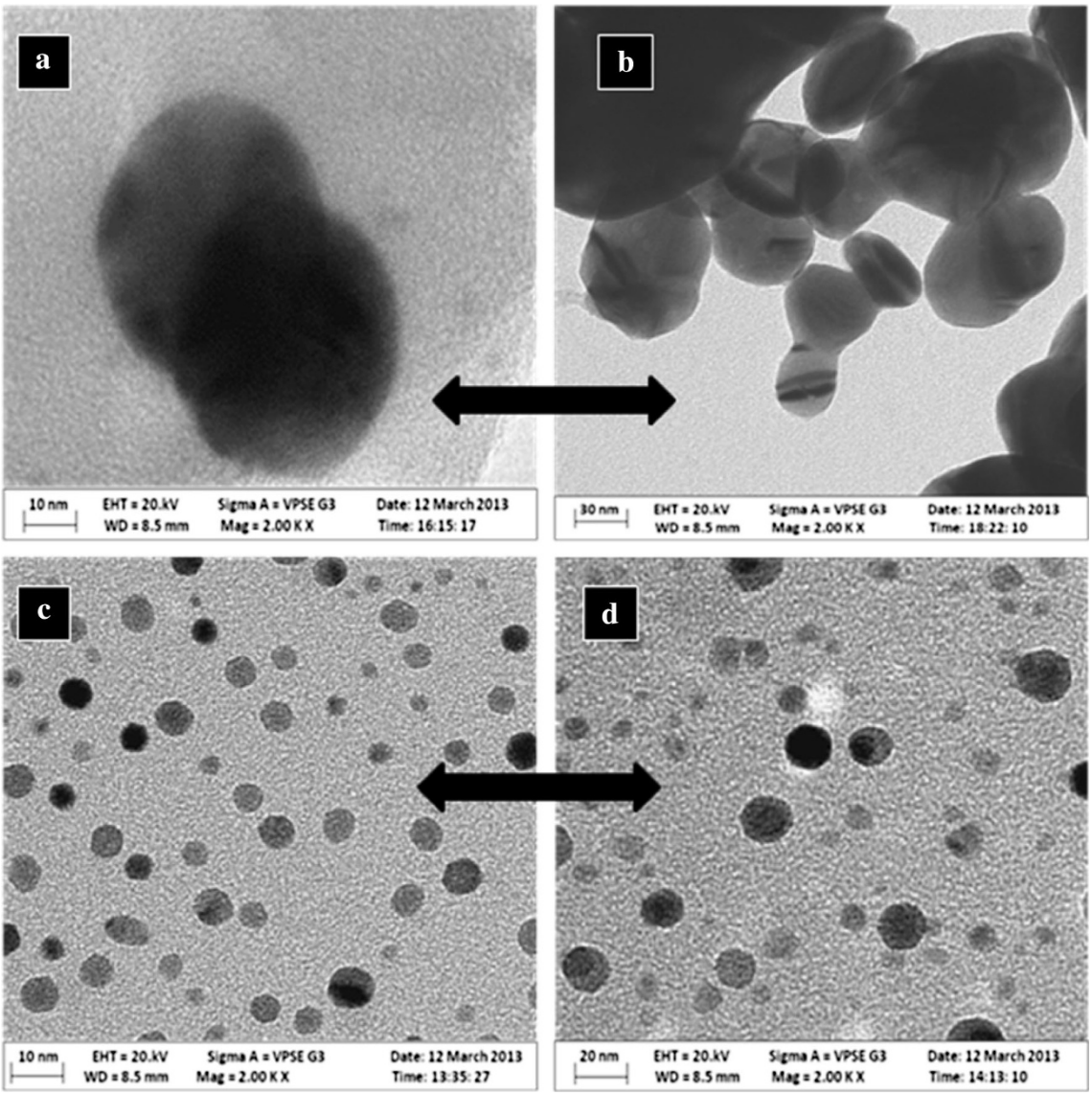

Fig. 4 Representative TEM images of nanosilver under Ao and Am-influenced synthesis

Hence, these results underscore the importance of biological extracts vis-à-vis their inherent biomolecular bioreducing agent as potential veritable tool for other metal structural evolution. Indeed, it serves to provide an alternative analytical platform for the screening of biomolecular phytochemical properties of biological extracts.

Mechanism and growth kinetics of SNP formed from the plant extracts

Since understanding of the mechanism and kinetics of nanoparticle formation, starting from an initial homogeneous aqueous solution is considered a yardstick for tuning particle synthesis towards a desirable size and morphology, we approached growth kinetics of the bioreduction process following Lifshitz–Slyozov–Wagner (LSW) model for coarsening which provides time dependence of the particle size and size distribution [37, 38].

Based on our TEM results which are more or less spherical, our first approach utilizes Ostwald Ripening (OR) Thompson–Freundlich model Eqs. (1) and (2). The general kinetic equation for these cases as diffusion-controlled OR is expressed as:

$$d^3 - d_0^3 = k_{\mathrm{OR}} t \tag{1}$$

Similarly,

$$r^3 - r_0^3 = k_{\mathrm{OR}} t \tag{2}$$

where d^3 is the cube of average diameter at time t, d_o^3 is the cube of initial particle diameter, and k_{OR} is the rate constant for OR given by [39–41]

$$k_{OR} = \frac{8\sigma D(V_m N_A)^2 C_s}{9RT} \quad (3)$$

To test whether the growth of SNPs in bioreduction system follows the well-known OR process, as it has been established for the growth of various metals and inorganic in solution phase system, we plotted particle diameter versus time [39, 40]. The representative plots in Fig. 5 displayed linear behaviour in all cases indicating that size increases with time. The phenomenon has also been proved by the time-resolved UV–Vis absorption spectrum in Fig. 1.

Since Figs. 1 and 5 and their analogy is not a satisfactory evidence of their compliance with OR growth mechanism as previously explained, we decided to seek for a more realistic validation by plotting particle r^3 as a function of time following Eq. (2) [41].

In most cases (Ao, Pg, Nl, Gl, Pig and Xa), the linear dependence as shown in the representative plots (Figs. 6, 7) indicate that the particle growth of SNPs is dominated by diffusion-limited coarsening, which is in compliance with OR growth mechanism. Initially, a solution comprising Ag^+ ion and homogenous plant extract will contain a large number of small particles. The smaller particles, therefore, act as "nutrients" for bigger particles and the average size increases. The rate of this process which is diffusion controlled decreases as the particles grow to its maximum as the case is for Ao (9 nm), Pg (14 nm), Nl (8 nm), Gl (17 nm) and Pig (33 nm) (Table 2)-mediated synthesis producing predominantly spherical morphology as revealed by the representative TEM images (Fig. 4c, d).

The discrepancies in the observed average maximum sizes obtained (Table 2) in different plant extracts of the same time-resolved (2 min minimum nucleation and growth time) program could be attributable to physiochemical, phytochemical and cytotoxicity of individual plant extracts as previously revealed [19, 20].

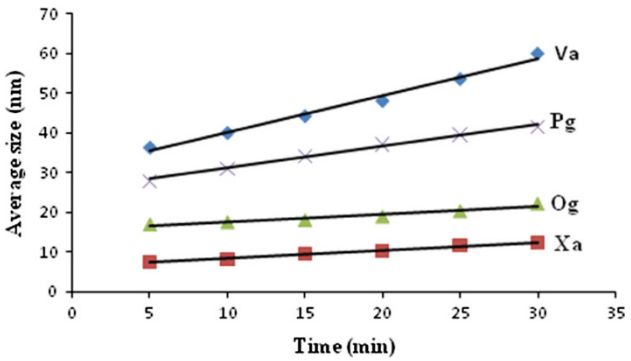

Fig. 5 Representative plots of average size against time for selected plant-mediated synthesis of silver nanoparticles

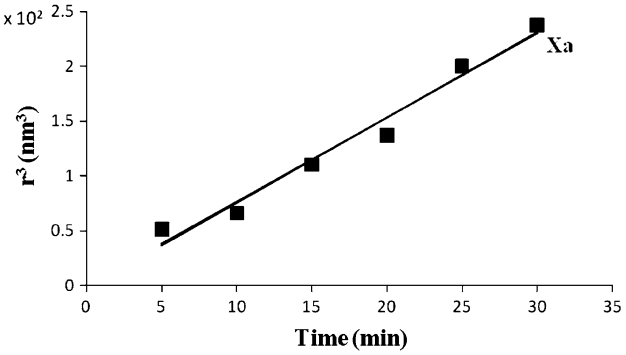

Fig. 6 Cube of SNP radius (r^3) plotted against growth time for Xa-mediated synthesis

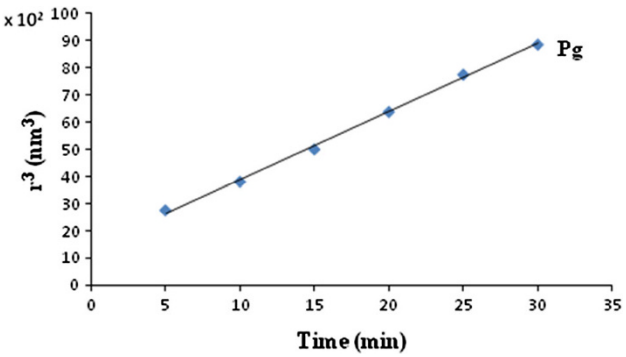

Fig. 7 Cube of SNP radius (r^3) plotted against growth time for Pg-mediated synthesis

However, it was observed that PBR of the SNPs produced via these plant extracts remain as expected (Fig. 1) without any significant shifting [7]. It is interesting, however, to note that most of the reaction initiated by these plant extracts underwent relatively fast reaction and nucleation process characterized by high rate constant (Table 2). The scenario displayed further suggest that these reaction conditions favour a growth rate more akin to the OR process, being predominantly controlled by diffusion without prejudice to the expected passivating influence of the organic inherent in the plant extracts [6].

However, in the case of Am, Og, Cc and Va, plots of r^3 versus time, to a limited extent deviated from linearity. A close look at the representative Figs. 7 and 8 for Og and Va-mediated bioreduction, respectively, expresses an initial linearity style of OR while other parts display non-linearity. These results importantly suggest dual mechanism with the involvement of diffusion-controlled (OR) and surface adsorption control mechanism (OA) which proceeds in succession. It follows that OR precedes OA with final emanation of a defect controlled quazi-spherical amidst some twinned structures (Fig. 4b). Under general conditions OR and OA growth mechanism occur

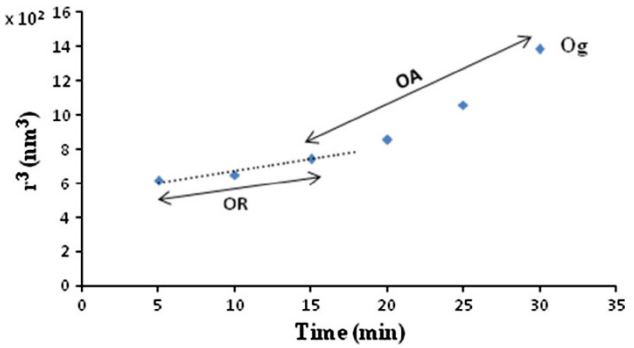

Fig. 8 Cube of SNP radius (r^3) plotted against growth time for Og mediated synthesis (note that initial 10 min growth time is linear and the remaining 15 min is non linear)

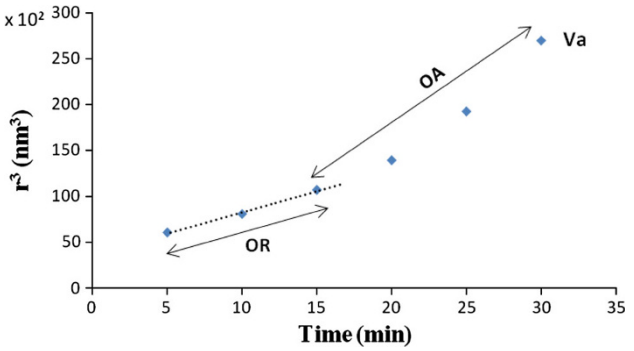

Fig. 9 Cube of SNP radius (r^3) plotted against growth time for Va-mediated synthesis (note that initial 10 min growth time is linear and the remaining 15 min is non-linear)

simultaneously and sometimes accompanied with the phase transformation [42, 43]. Illustratively, Fig. 10a expresses particle growth via coarsening and volume diffusion of ion giving credence to OR mechanism.

Illustration in Fig. 10b expresses OA formed via a spontaneous self-organization of adjacent particles, as effected by the capped organic on the surface producing quazi-spherical and twinned structure (Fig. 4) which are relatively of large sizes. However, under a strong and stable surface adsorption, OA stage may hold for a longer time producing unexpected large sizes [44]. For the plot in Fig. 8 under Og-influenced bioreduction, the initial stage, which is the time (10 min) it took for display of linearity has been considered as transition time; non linear behaviour took up to 15 min. Similar occurrence is displayed (Fig. 9) under Va influence. Previous work, however, in a chemical and physical synthetic approach, observed similar transition between OR → OA or OA → OR [37]. After the transition period, the effect of strong surface adsorption of the organic ($CH_3CO_2^-$) inherent in the plant extracts Am, Og, Cc and Va is plausibly considered to be the key to thermodynamically hinder the OR growth in the initial stage and which prompted OA action in the latter stage. Reports in the literature revealed that surface adsorption of anions (i.e.Br^-, $CH_3CO_2^-$) or (ClO_4^-) on the nanoparticles can slow down the OR growth rate [45, 46]. Even though, surface attachment concepts leading to OA remain a debatable issue in the literature [44–46]. However, it might be necessary to ascribe the dual mechanism (OR → OA) displayed in an unexpected direction to coarsening/assembly rather than supposedly nucleation/growth process. In solution phase synthesis, process such as coarsening and aggregation can compete with nucleation and growth producing unexpected large sizes of nanoparticles [46].

Naturally, one would expect all the bioreduction process mediated by plant extracts to follow the same pattern of growth since all of them contain organic passivating agent that supposedly should initiate surface adsorption coarsening process. In this report, we have not been able to provide reason for the unexpected. However, it has been revealed that the advance of OA growth kinetics (Fig. 10) depends on the understanding of the mechanism and whether the passivating agent is strong or weak [42–44]. For the weak one, during coarsening at high reaction temperature, it can be desorbed into water hindering the expected existence of OA. Under a more strong and stable surface adsorption, OA stage may hold longer leading to the unexpected large sizes nanoparticles as in the cases of Am (27 nm), Og (19 nm), Cc (41 nm) and Va (53 nm) (Table 2) bioreduction process. Therefore, in addition to coarsening, particle sizes can be varied by epitaxial attachment of one or more primary particles leading to the formation of secondary particles and eventual formation of irregularly shaped nanostructures [46]. It is noteworthy in these cases of dual mechanism (OR + OA) that their PBR are red-shifted which is an indication of surface adsorption on nanocrystal in a relatively slow reaction rate. SNP exhibiting red shifting of its PBR has been noted for their device application in optics and optoelectronic [33].

Conclusion

In an attempt to widen the scope of naturally, environmentally benign and easily available bioresourceable greens for the synthesis of metal nanoparticles, we have screened biodiversified plant extracts and looked into their capability for the synthesis of SNPs. Most of the plant-mediated bioreductions in this work are been studied for the first time. It is noteworthy that, with the aid of UV–Vis spectroscopy as time-resolved monitoring device, a number of the extract demonstrated unprecedented fast bioreduction reaction onset activity promptly within the first 2 min accompanied with fast reaction rate. There were cases of

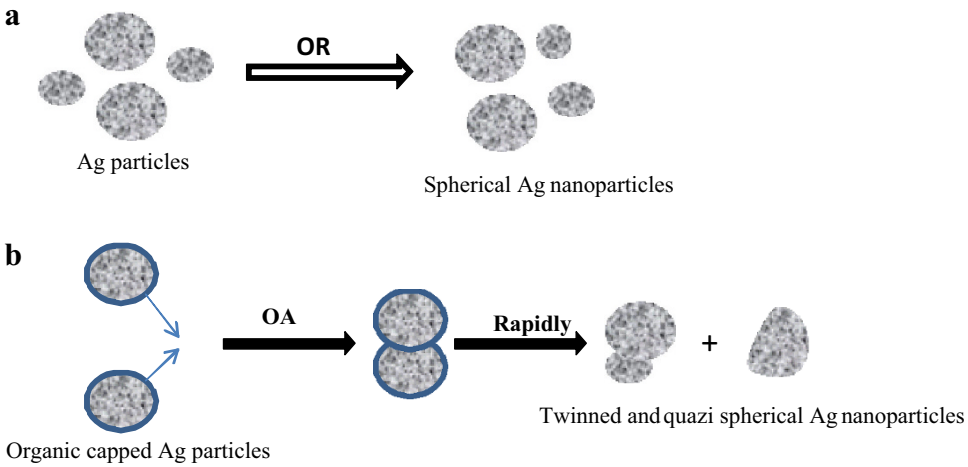

Fig. 10 Illustrative scheme of the growth kinetics in green system **a** Ostwald ripening model, **b** oriented attachment model

red shift in the observed PBR wavelengths as indication of cappings from organics inherent in the bioextracts.

Furthermore, we have engaged the combination of both TEM and time-resolved UV–Vis to monitor and predict the growth kinetic mechanism of SNPs synthesized from biodiversified plant extracts. The experimental data were analysed within the framework of the existing coarsening and particle growth mechanism, i.e. OR and OA. Based on the prior timescale analysis of the individual events, we proposed for some plant extracts' (Ao, Pg, Nl, Gl, Pig and Xa) bioreduction a single-stage time-sequenced description which follows nucleation of SNPs and its growth by diffusion control that complies with OR by virtue of linearity experience in a r^3 versus time plot.

However, a two-stage growth mechanism has been proposed for another set of plant extract (Am, Og, Cc and Va)-mediated synthesis which involves (1) an intermediate transition diffusion controlled via OR and finally surface adsorption of organic passivating agent by OA. In this case, coarsening and assembly processes are likely.

Indeed, this is the first preliminary demonstration through green experimental protocol of the ability to predict the coarsening of silver nanostructure evolution via OR or OR + OA. In principle, the proposed mechanistic framework, hopefully, provides underlying guides for tracking other nanostructure evolution in a green environment.

Acknowledgments The authors wish to acknowledge the Vice Chancellor of Federal University Lafia, Prof. Ekanem Ikpi Braide, Dean Faculty of Science, Prof. Martin Ogbe for creating an enabling environment for innovation and research. We are also grateful to the entire Staff of Chemistry, Microbiology and Physics Department for their support during the course of this research work. Special thanks also go to Mr. Danjuma Saidu, Mr Osuagwu Stanislaus and his team for their technical support. Prof. P. Kalu of Florida State University, USA and Shitole Joseph of iThemba Labs, South Africa are acknowledged for assistance in the running of some TEM.

References

1. Schultz, S., Smith, D.R., Mock, J.J., Schultz, D.A.: Single-target molecule detection with nonbleaching multicolor optical immunolabels. Proc. Natl. Acad. Sci. **97**, 996–1001 (2000)
2. Thirumurugan, G., Shaheedha, S.M., Dhanaraju, M.D.: In vitro evaluation of antibacterial activity of silver nanoparticles synthesized by using *Phytophthora infestans*. Int. J. Chemtech. Res. **1**, 714–716 (2009)
3. Bawendi, M.G., Steigerwald, M.L., Brus, L.E.: The quantum mechanics of larger semiconductor clusters ("Quantum Dots"). Annu. Rev. Phys. Chem. **41**, 477–496 (1990)
4. Xia, Y., Rogers, J.A., Paul, K.E., Whitesides, G.M.: Unconventional methods for fabricating and patterning nanostructures. Chem. Rev. **99**, 1823–1848 (1999)
5. Sharma, V.K., Yngard, R.A., Lin, Y.: Silver nanoparticles: green synthesis and their antimicrobial activities. Adv. Colloid interf. Sci. **145**, 83–96 (2009)
6. Awwad, A.M., Nida, M.S., Amany, O.A.: Green synthesis of silver nanoparticles using carob leaf extract and its antibacterial activity. Int. J. Ind. Chem. **4**, 1–6 (2013)
7. Harekrishna, B., Dipak, K.B., Gobinda, P.S., Priyanka, S., Santanu, P., Ajay, M.: Green synthesis of silver nanoparticles using seed extract of *Jatropha curcas*. Colloids Surf. A Physicochem. Eng. Asp. **348**, 212–216 (2009)
8. Satyavani, K., Ramanathan, T., Gurudeeban, S.: Green synthesis of silver nanoparticles by using stem derived callus extract of bitter apple (*Citrullus colocynthis*). Dig. J. Nanomater. Biostruct. **6**, 1019–1024 (2011)
9. Shankar, S.S., Rai, A., Ahmad, A., Sastry, M.: Rapid synthesis of Au, Ag, and bimetallic Au core–Ag shell nanoparticles using neem (*Azadirachta indica*) leaf broth. J. Colloid Interf. Sci. **275**, 496–502 (2004)
10. Vilchis-Nestor, A.R., Sanchez-Mendieta, V., Camacho-Lopez, M.A., Gomez-Espinosa, R.M., Camacho-Lopez, M.A., Arenas-Alatorre, J.A.: Solventless synthesis and optical properties of Au and Ag nanoparticles using *Camellia sinensis* extract. Mater. Lett. **62**, 3103–3105 (2008)

11. Swarnalatha, L., Christina, R., Shruti, R., Payas, B.: Evaluation of invitro antidiabetic activity of Sphaeranthus amaranthoides silver nanoparticles. Int. J. Nanomater. Biostruct. **2**, 25–29 (2012)
12. Bharani, M., Thirunethiran, K., Varalakshmi, B., Gayathiri, G., Lakshmi, P.K.: Synthesis and characterization of silver nano particles from *Wrightia tinctoria*. Int. J. Appl. Biol. Pharm. Technol. **3**, 58–63 (2012)
13. Chandran, N., Padmanaban, S., Sahadevan, R.: Green synthesis of silver nanoparticles using *Datura metel* flower extract and evaluation of their antimicrobial activity. Int. J. Nanomater. Biostruct. **2**, 16–21 (2012)
14. He, S.Y., Guo, Z.R., Zhang, Y., Zhang, S., Wang, J., Gu, N.: Biosynthesis of gold nanoparticles using the bacteria *Rhodopseudomonas capsulata*. Mater. Lett. **61**, 3984–3987 (2007)
15. Adaramoye, O.A., Akintayo, O., Fafunso, M.A.: Lipid lowering effects of methanolic extract of *Vernonia amygdalina* leaves in rats fed on high cholesterol diet. Vasc. Health Risk Manag. **4**, 235–241 (2008)
16. Okwu, D.E.: Phytochemicals, vitamins and mineral contents of two Nigerian medicinal plants. Int. J. Mol. Med. Adv. Sci. **1**, 375–381 (2005)
17. Kimura, S., Tamaki, T., Aoki, N.: Acceleration of fibrinolysis by the N-terminal peptide of alpha 2-plasmin inhibitor. Am. Soc. Hematol. **66**, 157–160 (1985)
18. Qian, H., Nihorimbere, V.: Antioxidant power of phytochemicals from *Psidium guajava* leaf. J. Zhejiang Univ. Sci. **5**, 676–683 (2004)
19. Tanko, Y., Kamba, B., Saleh, M.I.A., Musa, K.Y., Mohammed, A.: Anti-nociceptive and anti-inflammatory activities of ethanolic flower extract of *Newbouldia laevis* in mice and rats. Int. J. Appl. Res. Nat. Prod. **1**, 13–19 (2008)
20. Usman, H., Osuji, J.C.: Phytochemical and in vitro antibacterial assay of the leaf extract of *Newbouldia laevis*. Afr. J. Tradit. CAM **4**, 476–480 (2007)
21. Aboua, L.R.N., Seri-Kouassi, B.P., Koua, H.K.: Insecticidal activity of essential oils from three aromatic plants on *Callosobruchus maculatus* F. in Côte D'ivoire. Eur. J. Sci. Res. **39**, 243–250 (2010)
22. Okafor, J.C., Okolo, H.C., Ejiofor, M.A.N.: Strategies for enhancement of utilization potential of edible woody forest species of south-eastern Nigeria. In: The Biodiversity of African Plants, pp. 684–695. Kluwer, The Netherlands (1996)
23. Wang, D.S., Xie, T., Li, Y.D.: Nanocrystals: solution based synthesis and applications as nanocatalysts. Nano Res. **2**, 30–46 (2009)
24. Shingu, P.H.: Mechanical alloying. Mat. Sci. Forum. 88–90 (1992)
25. Forough, M., farhadi, K.: Biological and green synthesis of silver nanoparticles, Turkish. J. Eng. Environ. Sci. **34**, 281–287 (2010)
26. Elemike, E.E., Chuku, A., Labulo, A.H., Oseghale, C.O., Owoseni, M.C., Mfon, R., Dare, O.E., Adesuji, E.T.: Evaluation of antibacterial activities of silver nanoparticles green-synthesised using pineapple leaf (*Ananas comosus*). Micron **57**, 1–5 (2014)
27. Embden, J.V., Sader, J.E., Dadivson, M., Mulvaney, P.: Evolution of colloidal nanocrystals: theory and modeling of their nucleation and growth. J. Phys. Chem. C **113**, 16342 (2009)
28. Viswanatha, R., Santra, P.K., Dasgupta, C., Sarma, D.: Growth mechanism of nanocrystals in solution: ZnO, a case study. Phys. Rev. Lett. **98**, 255501 (2007)
29. Penn, R.L., Banfield, J.F.: Imperfect oriented attachment: dislocation generation in defect-free nanocrystals. Science **281**, 969–971 (1998)
30. Anastas, P.T., Kirchhoff, M.M.: Origins, current status, and future challenges of green chemistry. Acc. Chem. Res. **35**(9), 686–694 (2002)
31. Ponarulselvam, S., Panneerselvam, C., Murugan, K., Aarthi, N., Kalimuthu, K., Thangamani, S.: Synthesis of silver nanoparticles using leaves of *Caranthus roseus* linn. G. Don and their antiplasmodial activities. Asian Pac. J. Trop. Med. **2**, 574–580 (2012)
32. Velicov, K.P., Zegers, G.E., Blaaderem, V.: Synthesis and characterization of large colloidal silver particles. Langmuir **19**(4), 1384–1389 (2003)
33. Smith, A.M., Duan, H., Rhyner, M.N., Ruan, G., Nie, S.A.: A systematic examination of surface coatings on the optical and chemical properties of semiconductor quantum dots. Phys. Chem. **8**, 3895–3903 (2006)
34. Huang, J., Li, Q., Sun, D., Lu, Y., Su, Y., Yang, X., Wang, H., Wang, Y., Shao, W., He, N., Hong, J., Chen, C.: Biosynthesis of silver and gold nanoparticles by novel sundried *Cinnamomum camphora* leaf. Nanotechnology **105104**, 18 (2007)
35. Kumar, V., Kumar, S.: Plant-mediated synthesis of silver and gold nanoparticles and their applications. J. Chem. Technol. Biotechnol. **84**, 151–157 (2008)
36. Dare, E.O., Makinde, O.W., Ogundele, K.T., Osinkolu, G.A., Fasasi, Y.A., Sonde, I., Bamgbose, J.T., Maaza, M., Sithole, J., Ezema, F., Adewoye, O.O.: Zinc salt mediated synthesis, growth kinetic, and shaped evolution of silver nanoparticles. ISRN Nanomater. (2012). doi:103402/2012/376940
37. Arunasish, L., Gargi, M., Archana, S., Marina, S., Subhabrata, D., Arindam, C., Rajdip, B.: A generalized three stage mechanism of ZnO nanoparticle formation in homogenous liquid medium. J. Phys. Chem. C **116**, 24757–24769 (2012)
38. Lifshitz, J.M., Slyozov, V.V.: The kinetics of precipitation from supersaturated solid solutions. J. Phys. Chem. Solids **19**, 35–50 (1961)
39. Kimijima, K., Sugimoto, T.: Growth mechanism of AgCl nanoparticles in a reverse micelle system. J. Phys. Chem B **108**, 3735–3738 (2004)
40. Wilcoxon, J.P., Provencio, P.: Etching and aging effects in nanosize Au clusters investigated using high-resolution size-exclusion chromatography. J. Phys. Chem B **107**(47), 12949–12957 (2003)
41. Gerko, O., Abhinav, N., Penn, L., Peter, S.: The growth kinetics of TiO_2 nanoparticles from titanium(IV) alkoxide at high water/titanium ratio. J. Phys. Chem B **107**, 1734–1738 (2003)
42. Jing, Z., Feng, H., Zang, L.: Progress of nanocrystalline growth kinetics based on oriented attachment. Nanoscale **2**, 18–34 (2010)
43. Huang, F., Zhang, H., Banfield, J.F.: The role of oriented attachment growth in hydrothermal coarsening of nanocrystalline ZnS. J. Phys. Chem B **107**, 10470–10475 (2003)
44. Zhang, J., Wang, Y., Zheng, J., Huang, F., Chen, D., Lang, Y., Ren, G., Lin, Z., Wang, C.: Oriented attachment kinetic for ligand capped nanocrystals: coarsening of thiol-PbS nanoparticles. J. Phys. Chem. B **111**, 1449–1454 (2007)
45. Hu, Z., Oskan, G., Penn, R.L., Pesika, N., Searson, P.C.: The influence of anion on the coarsening kinetic of ZnO nanoparticles. J. Phys. Chem. B **107**, 3124–3130 (2003)
46. Oskam, G., Hu, Z., Penn, R.L., Pesika, N., Searson, P.C.: Coarsening of metal oxide nanoparticles. Phys. Rev. E Stat. Nonlinear Soft Matter Phys. **66**, 01403 (2002)